IMR KINKEN Research Highlights 2016

Infrastructural Materials

IMR KINKEN Research Highlights 2016

Enhanced Surface Hardening in Nitriding Process by Dynamic Provision of Nucleation Site For Alloy Nitride Precipitation

Higher surface hardness is required for machinery parts to ensure high reliability and longer life. We found that the combined addition of vanadium and aluminum to iron for nitriding treatment resulted in a significant increase in surface hardness because the vanadium–nitrogen atoms form fine clusters in the early stage and aluminum nitride precipitation is enhanced by the nucleation at the cluster.

Machinery parts such as gears and shafts require high toughness, as well as high hardness, for resistance to wear and fatigue. However, in general, those properties cannot be improved simultaneously. Therefore, surface-hardening processes are performed to harden only the surface region, while the inward region remains ductile. Nitriding is one of the most popular surface-hardening treatments for steel, which improves fatigue-, wear- and corrosion-resistant properties. As compared to other surface-hardening processes, nitriding has advantages in terms of small distortion during the process, higher surface hardness, and better softening resistance at elevated temperatures. The process has thus attracted much attention for the surface hardening of high-precision parts. In the nitriding process, steel parts are held at 500–600°C in a nitriding atmosphere so that nitrogen atoms are absorbed from the surface and then diffuse inward. Surface hardening by nitriding is caused mainly by precipitation of fine alloy nitrides or of alloying element (M)–nitrogen (N) clusters near the surface. Therefore, an understanding of alloy nitride precipitation behavior is crucial to controlling surface hardening by nitriding.

In order to clarify alloying effects on the precipitation of alloy nitrides and the resultant surface hardening, we investigated the microstructure and surface hardness of various nitrided Fe–M binary alloys [1]. It was found that nano-sized M–N clusters formed in the nitriding of Fe–V or Fe–Ti alloys, whereas no precipitation of Al nitrides was observed [1]. As a result, the Fe–Al alloy did not show surface hardening as compared to the other alloys, as shown in Fig. 1 (top). Because Al is also a strong nitride-forming element, its precipitation should be facilitated by introducing nucleation sites.

Recently, we investigated the effects of the combined addition of Al and V atoms, and we found that the addition of V to Fe–Al alloys significantly accelerated the precipitation of Al nitrides, resulting in significant surface hardening [Fig. 1 (top)]. Because the V–N attractive interaction is much stronger than the Al–N one, the formation of V–N clusters take place first, and then precipitation of Al nitrides is induced by nucleation at the V–N cluster/matrix interface at the growth front of the nitrided region [Fig. 1 (bottom)]. Consequently, such dynamic provision of nucleation sites during the nitriding process was found to be very effective for enhanced surface hardening.

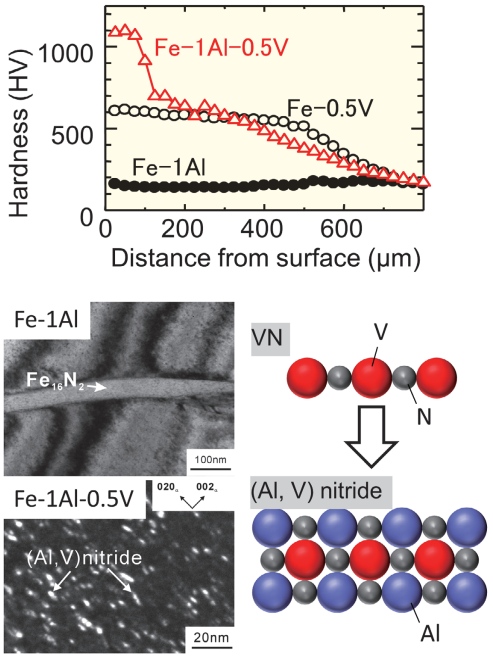

Fig. 1 (top) Hardness–depth profiles of the specimen nitrided at 550°C for 16 h, (bottom left) TEM images of precipitates in Fe–1Al and Fe–1Al–0.5V alloys, and (bottom right) schematic illustration of nucleation of Al nitride at the V–N cluster.

References

[1] G. Miyamoto, Y. Tomio, H. Aota, K. Oh-ishi, K. Hono, and T. Furuhara, Mater. Sci. Technol., **27**, 742 (2011).

[2] G. Miyamoto, S. Suetsugu, K. Shinbo, and T. Furuhara, Metall. Mater. Trans. A, **46A**, 5011 (2015).

Keywords: steel, atom probe tomography, nanocluster

Goro Miyamoto (Microstructure Design of Structural Metallic Materials Division)
E-mail: miyamoto@imr.tohoku.ac.jp
URL: http://www.st-mat.imr.tohoku.ac.jp/en/index.html

Local Structure around Ge in Lithium– Germanate Glasses

The local structure around Ge in lithium–germanate glasses was investigated by using the anomalous X-ray scattering technique. The averaged coordination number of the first neighboring Ge–O pair increased with increasing Li_2O content up to 24 mol%. The introduction of an octahedral GeO_6 unit is one of the most fundamental structural changes accompanying the so-called germanate anomaly detected in density measurements.

The densities of lithium–germanate glasses show a maximum value at approximately 20 mol% Li_2O [1, 2]. Because the physical properties of glasses correlate with their atomic structures, several advanced analytical studies have been applied for elucidating the structural model for this interesting behavior. We investigated the local structure around Ge in lithium-germanate glasses using anomalous X-ray scattering (AXS) measurements, which is ranked as the most advanced method currently available for obtaining quantitative local structural information for glasses [3].

Lithium–germanate glass samples were prepared by an ordinary melt–quench technique. Powder mixtures of GeO_2 (99.99%) and Li_2CO_3 (99.0%) were calcined at 923 K for 1 h. The prepared samples were melted in a platinum crucible in air for 1 h at 1673 K, and then the melts were quenched by pressing them between two copper plates. The AXS measurements at the Ge *K* absorption edges were performed at the BL-7C beamline of the Photon Factory at the Institute of Material Structure Science, High Energy Accelerator Research Organization.

Figure 1 shows the $\Delta Qi_{Ge}(Q)$ profiles [4] of four lithium–germanate glasses. Significant differences are observed at the first peak region of approximately 1.8 $Å^{-1}$, and the peaks decrease and broaden as the Li_2O content increases. Because the first peak is associated with the structure of Ge–Ge pairs, the change detected in the $\Delta Qi_{Ge}(Q)$ profiles suggests the possible breakdown of the network structure composed of GeO_4 tetrahedra.

The environmental RDFs for Ge calculated by Fourier transformation of the $\Delta Qi_{Ge}(Q)$ profiles indicated that the distance of the Ge–O pairs increased with increasing Li_2O content. This suggests the introduction of a new local structural unit of GeO_6, as shown in a previous work. Further analysis showed that the fraction of GeO_6 in the lithium–germanate glasses increased with increasing Li_2O content up to 24 mol%. This variation in local structural unit produced a slightly different

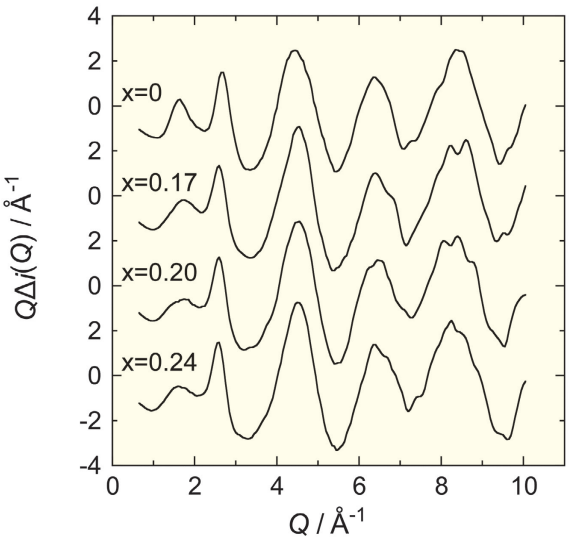

Fig. 1 shows environmental interference functions of $xLi_2O - (1 - x)GeO_2$ glasses.

behavior, which was suggested originally by the density measurements. Nevertheless, a similar suggestion was also reported by Henderson and Fleet [5] through a discussion of the observed change in Ge–O distances.

References

[1] A. O. Ivanov and K. S. Evstropiev, Dokl. Akad. Nauk SSSR **145,** 797 (1962).
[2] M. K. Murthy and J. Ip, Nature **201**, 285 (1964).
[3] Y. Waseda, E. Matsubara, and K. Sugiyama, Sci. Rep. RITU **A34**, 1 (1988).
[4] H. Arima, T. Kawamata, and K. Sugiyama, J. Min. Pet. Sci. **110**, 60 (2015).
[5] G. S. Henderson and M. E. Fleet, J. Non-Cryst. Solids. **134,** 259 (1991).

Keywords: glass, anomalous X-ray scattering, XAFS
Hiroshi Arima and Kazumasa Sugiyama (Chemical Physics of Non-Crystalline Materials Division)
E-mail: arimah@imr.tohoku.ac.jp
URL: http://www.xraylab.imr.tohoku.ac.jp/

Effect of Solid-solute Oxygen Addition on Wear Properties of Biomedical Ti–29Nb–13Ta–4.6Zr Alloy

Ti–29Nb–13Ta–4.6Zr alloy (TNTZ) exhibits good biological and mechanical compatibilities owing to its low toxicity and the fact that its Young's modulus is close to that of human bone (approximately 60 GPa). Although the wear resistance of titanium alloys is generally poor as a biomaterial, the mechanical strength of TNTZ can be improved by adding an interstitial element, oxygen (O). Thus, the wear characteristics of TNTZ with different oxygen contents were investigated. The volume loss of TNTZ with high O content was significantly lower than that of TNTZ with low O content. Therefore, it is concluded that solid-solution strengthening by oxygen increases the wear resistance of TNTZ.

Wear resistance is one of the most important material properties for biomedical devices with metal-to-metal contact parts because failure can easily occur at such contact parts.

The wear behaviors and mechanisms of two types of titanium alloys were previously analyzed and compared both in air [1] and in Ringer's solution [2]. The first alloy was a conventional (α + β)-type Ti–6Al–4V extra-low-interstitial (Ti64) alloy; the second was a newly developed β-type Ti alloy for biomedical applications, Ti–29Nb–13Ta–4.6Zr (TNTZ). It was concluded that volume losses (V_{loss}) of the TNTZ discs and balls were larger than those of the respective Ti64 discs and balls, both in air and in Ringer's solution. Particularly, when the TNTZ disc slid against the TNTZ ball, V_{loss} of both the disc and ball exhibited maximum values both in air and in Ringer's solution. These results are related to the severe subsurface deformation of TNTZ, which is caused by the lower resistance of TNTZ to plastic shearing than Ti64, inducing delamination and resulting in a higher wear rate.

Therefore, it is necessary to increase the wear resistance of TNTZ while keeping its Young's modulus similar to that of human bone. Young's modulus is related to the crystal structure, which remains essentially unchanged with increasing interstitial element content. Thus, interstitial elements are very promising because their addition to TNTZ is expected to improve its plastic shear resistance via solution strengthening. The wear behavior of TNTZ with oxygen contents of 0.06 and 0.89 mass% (06O and 89O, respectively) were investigated in this study.

The Vickers hardness values of discs and balls made of Ti64, 06O, and 89O were measured. The hardness of the 89O discs was higher than that of the Ti64 discs. Moreover, the hardness of the 89O balls was higher than that of the Ti64 balls. In the case of the 06O material, the hardness of both discs and balls was lower than that of the respective Ti64 and 89O discs and balls.

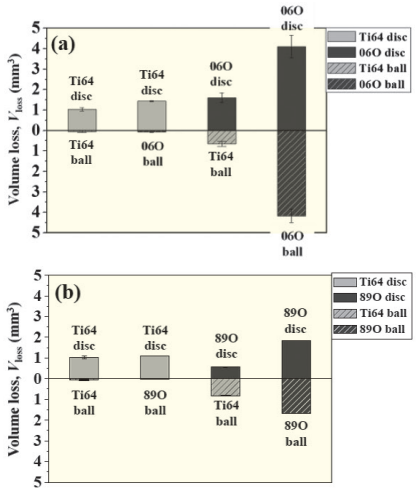

Fig. 1 Volume losses of (a) Ti64/06O combinations and (b) Ti64/89O combinations during frictional wear tests in Ringer's solution.

The V_{loss} values of discs and balls made of Ti64, 06O, and 89O subjected to frictional wear tests in Ringer's solution are shown in Fig. 1. The V_{loss} values of the 89O discs and balls are much lower than those of the 06O discs and balls, regardless of the mating materials. The increase in hardness improved the plastic shear resistance of the 06O discs and balls, which is necessary to avoid severe delamination wear. Therefore, it can be concluded that solid-solution strengthening is a very effective treatment for improving the wear resistance of TNTZ biomedical implants.

References

[1] Y.-S. Lee, M. Niinomi, M. Nakai, K. Narita, and K. Cho, J. Mech. Behav. Biomed. Mater. **41**, 208 (2015).

[2] Y.-S. Lee, M. Niinomi, M. Nakai K. Narita, and K. Cho, Mater. Trans. **56**, 317 (2015).

Keywords: alloy, biological, mechanical properties
Mitsuo Niinomi (Biomaterials Science Division)
E-mail: niinomi@imr.tohoku.ac.jp
URL: http://biomat.imr.tohoku.ac.jp/

Development of Eu:SrI2 Scintillator Single Crystal and Gamma-ray Detection Devices Using the Eu:SrI2 Bulk Single Crystal

High-light-yield and high-energy-resolution Eu:SrI2 gamma-ray scintillator single crystals were developed using a modified micro-pulling-down (μ-PD) method. In addition, Eu:SrI2 bulk single crystals with diameters of 1–2 in. were grown by a modified Bridgman method using a modified μ-PD furnace. Gamma-ray detection devices using the Eu:SrI2 bulk single crystal, such as a spectrometer were also developed.

Halide (chloride, bromide, and iodide) materials were investigated owing to their significant potential as scintillator materials with high light yield and high energy resolution. Halide materials have relatively small band-gaps as compared to oxides and fluorides, and the high light yield of halide materials is attributable to this small band-gap. In addition, the high light yield provides high-energy resolution. However, most halide materials have strong hygroscopicity, and it is difficult to grow high-quality and high-transparency single crystals.

Therefore, we developed a modified micro-pulling-down (μ-PD) method for the crystal growth of halide materials [Fig. 1(a)] [1]. In the modified μ-PD method, a removable chamber that can be entered through a glove box filled with high-purity Ar gas is used, thus protecting the inside of the chamber from exposure to outside atmosphere. Therefore, the modified μ-PD method can be used to grow single crystals of halide materials without being affected by outside atmosphere.

Using the modified μ-PD method, we grew Eu:SrI2 single crystals with high transparency. The light yield and energy resolution were also much higher than those of previous scintillator materials [2].

In addition, we developed a modified Bridgman method using the modified μ-PD furnace for the growth of bulk single crystals because the modified μ-PD method can grow only fiber single crystals. By the modified Bridgman method, we obtained 1 in. Eu:SrI2 bulk single crystals with various Eu concentrations [3]. By further optimization of the growth conditions, we grew 1.5 and 2 in. Eu:SrI2 bulk single crystals through collaboration with C&A Corporation [4]. We then developed radiation devices using the bulk Eu:SrI2 single crystal by the JST project.

Especially, a handheld high-performance spectrometer using the Eu:SrI2 bulk single crystal was developed in collaboration with Chiyoda Technology Corporation [Fig. 1(b)].

(a)

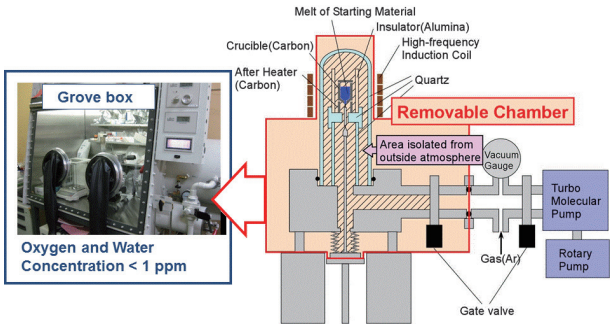

(b)

Fig. 1 (a) Schematic of the modified μ-PD method. (b) Spectrometer using Eu:SrI2 bulk single crystal.

References

[1] Y. Yokota, N. Kawaguchi, K. Fukuda, T. Yanagida, A. Yoshikawa, and M. Nikl, J. Cryst. Growth **318,** 908 (2011).

[2] Y. Yokota, K. Nishimoto, S. Kurosawa, D. Totsuka, and A. Yoshikawa, J. Cryst. Growth **375**, 49 (2013).

[3] Y. Yokota, S. Kurosawa, K. Nishimoto, K. Kamada, and A. Yoshikawa, J. Cryst. Growth **401**, 343 (2014).

[4] Y. Yokota, T. Ito, S. Yasuhiro, S. Kurosawa, Y. Ohashi, K. Kamada, and A. Yoshikawa, IEEE Trans. Nucl. Sci. (2016) accepted.

Keywords: crystal growth, devices, radiation effects
Akira Yoshikawa (Advanced Crystal Engineering Laboratory)
E-mail: yoshikawa@imr.tohoku.ac.jp
URL: http://yoshikawa-lab.imr.tohoku.ac.jp/index-e.html

Fine-Structured High-Temperature Non-Oxide Ceramics by Phase Decomposition via Spark Plasma Sintering and Heat Treatment

Transition-metal non-oxide ceramics are promising as ultra-high-temperature ceramics and high-hardness cutting tools. We synthesized dense compacts from Ti- and Zr-based carbide powders by spark plasma sintering, and nano–submicron-sized fine structures were assembled by the subsequent heat treatment. The formation of the self-assembled microstructures enhanced the hardness and toughness.

Ti- and Zr-based non-oxide materials such as TiC, ZrC, TiN, and ZrN have been receiving much attention for use in extremely severe environments, e.g., ultra-high temperature ceramics and cutting tools, because of their high melting point, excellent corrosion resistance, and high hardness. However, for practical use in industry, low sinterability and fracture toughness should be improved. It is difficult to consolidate Ti- and Zr-based non-oxide powders into dense compacts using conventional sintering techniques. In general, a small amount of metals such as Ni and Co is added to promote sintering; however, the metal additives degrade the mechanical properties and corrosion resistance of Ti and Zr carbides. As the powder manufacturing of non-oxide ceramics has developed, it has been of great interest to consolidate pure non-oxide powders and to design dense and high-strength bulk materials by controlling the micro- and nanostructures.

Spark plasma sintering (SPS) is a novel technique to quickly consolidate non-oxide ceramic powders at high temperatures. We consolidated TiC–ZrC composites from TiC and ZrC powders by SPS at sintering temperatures up to 2473 K. At high temperatures above 2273 K, (Ti, Zr)C solid solutions were formed with a fully dense and uniform morphology. Because these dense sintered bodies are pure non-oxide Ti–Zr carbides with no metal sintering additives, the Vickers hardness reached 26 GPa [1, 2]. The sintered bodies of the (Ti, Zr)C solid solutions decomposed into Zr-rich and Ti-rich phases by the subsequent heat treatment at temperatures lower than the sintering temperature (1573–2273 K) [3]. The phase decomposition resulted in the formation of fine nodular structures several tens to hundreds of nanometers in length, with the coherent crystal orientation relationship of the TiC-rich phase {100}//ZrC-rich phase {100}, as shown in Figs. 1(a) and (b). By detailing the effects of TiC–ZrC compositions and heat-treating conditions on the decomposition behavior, we discovered a variety of microstructures formed by self-assembling via eutectoid reactions and spinodal decomposition, as shown in Figs. 1(c) and (d). The formation of the fine microstructure enhanced the hardness and fracture toughness [4].

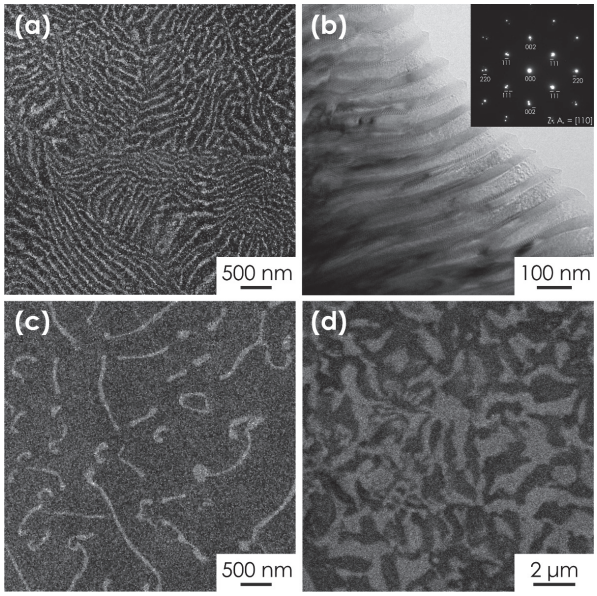

Fig. 1 Phase-decomposed microstructures of TiC–ZrC composites prepared by SPS and the subsequent heat treatment. (a): Fine nodular structure composed of Ti-rich (bright contrast) and Zr-rich (dark contrast) solid solutions. (b): TEM bright-field image and electron diffraction pattern of the several tens of nanometers nodular structure. (c) and (d): Nodular structure and labyrinth structure.

References

[1] Y. Li, H. Katsui, and T. Goto, Key. Eng. Mater. **616**, 52 (2014).
[2] Y. Li, H. Katsui, and T. Goto, Ceram. Int. **41**, 7103 (2015).
[3] Y. Li, H. Katsui, and T. Goto, Ceram. Int. **41**, 14258 (2015).
[4] Y. Li, H. Katsui, and T. Goto, J. Eur. Ceram. Soc. (2016) in press.

Keywords: ceramic, nanostructure, mechanical properties
Takashi Goto, Hirokazu Katsui and Akihiko Ito (Multi-Functional Materials Science Division)
E-mail: goto@imr.tohoku.ac.jp
URL: http://www.goto.imr.tohoku.ac.jp/

Regulating the Coarsening of γ′ Phase in Superalloys

Stabilizing the γ′ phase represents one of the key challenges in developing next-generation superalloys. We fabricated a cobalt-based superalloy with a nanoscale coherent γ′ phase, $(Ni,Co)_3(Al,Ti,Nb)$, isolated by stacking-fault ribbons in the alloy matrix as a result of Suzuki segregation of the alloying atoms. This new nanostructure can reduce the coarsening rate of the γ′ phase at high temperatures.

One key to preserving the large density of the nanoscale γ′ phase while inhibiting its coarsening at high temperatures is to single out an ideal microstructure that can effectively reduce the diffusion among γ′-phase particles without sacrificing the strength of the superalloy. The formation of planar stacking-fault ribbons in superalloys as a result of Suzuki segregation of the alloying elements may fulfill this role.

Here, we developed a new cobalt-based superalloy comprising 35% Ni, 17.5% Cr, 8% Mo, 3% Nb, 2% Al, and 0.8% Ti (mass%) [1]. After cold swaging, the alloy was subjected to aging at 1073 K for 3 h. The nanoscale γ′-phase particles precipitated in the γ matrix [Fig. 1 (a)], whereas the stacking-fault ribbons were formed because of Suzuki segregation of the alloying elements (*e.g.* Mo and Cr) into these planar defects [2, 3] [Fig. 1 (b)]. The enriched solute atoms (Suzuki segregation) hampered the diffusion of the major elements of the γ′ phase (Ni, Al, etc.) across these planar defects, thereby isolating individual γ′-phase nanoparticles and reducing the coarsening rate of the γ′ particles during high-temperature exposure [Figs. 1 (c) and (d)]. Furthermore, Suzuki segregation of alloying elements itself can serve as an important additional factor in strengthening superalloys at elevated temperatures (*e.g.* 973 K).

The developed cobalt-based superalloy demonstrated an extremely high strength of 1250 MPa at 973 K, as indicated in Fig. 2. As compared to commercial superalloys (*e.g.* Waspaloy®), the developed alloy showed higher yield stress both at room temperature and at elevated temperatures (Fig. 2). Therefore, the present strategy opens a new avenue in producing superalloys with extremely high structural stability at high temperatures and exceptional mechanical properties. In addition, the present alloy showed excellent cold workability. Thus, the application of this method in various structural applications, including heat-resistant springs, is expected.

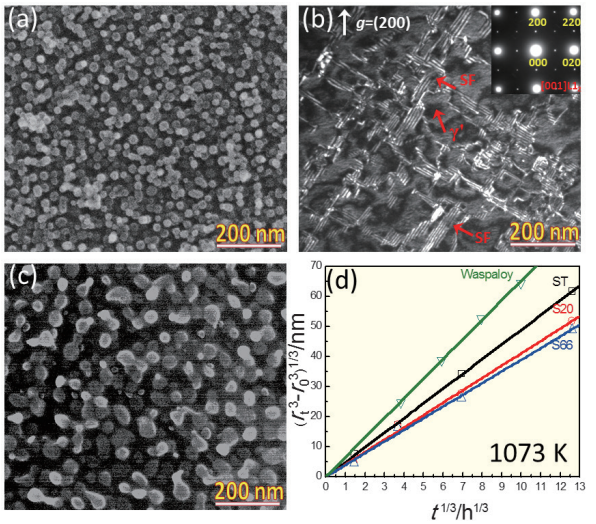

Fig. 1 (a) The morphology of γ′ phase in cold-swage alloy after aging, (b) stacking-fault ribbons, (c) the morphology of γ′ phase after aging for 2000 h, and (d) the LSW relationship of the coarsening γ′ phase [1].

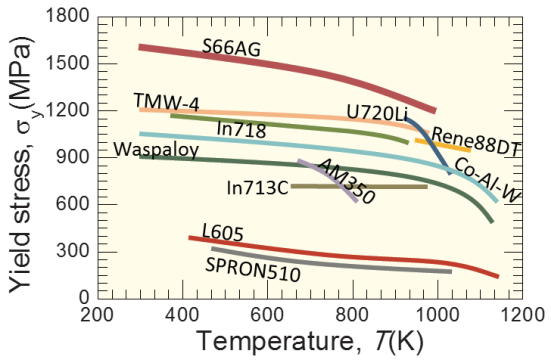

Fig. 2 The temperature dependence of yield stress of the present alloy (S66AG) [1]. The results are compared to those of commercial superalloys such as TMW-4, In718, Waspaloy®, and so on.

References

[1] H. Bian, X. Xu, Y. Li, Y. Koizumi, Z. Wang, M. Chen, K. Yamanaka, and A. Chiba, NPG Asia Mater. **7**, e212 (2015).
[2] Y. Koizumi, T. Nukaya, S. Suzuki, S. Kurosu, Y. Li, H. Matsumoto, K. Sato, and A. Chiba, Acta Mater. **60**, 2901 (2012).
[3] A. Chiba and M. S. Kim, Mater. Trans. **42**, 2112 (2001).

Keywords: alloy, nanostructure, mechanical properties
Akihiko Chiba (Deformation Processing Division)
E-mail: a.chiba@imr.tohoku.ac.jp
URL: http://www.chibalab.imr.tohoku.ac.jp/

Distinguishing Rare-earth Magnets Utilizing Portable Cathodoluminescence Spectrometer

We report a method to distinguish neodymium–iron–boron (NdFeB) and samarium–cobalt (Sm–Co) magnets using a portable cathodoluminescence (CL) spectrometer that we realized. Luminescence owing to the NdFeB and Sm–Co magnets was detected by capturing CL images of vacuum-dried residues of respective solutions containing the dissolved NdFeB and Sm–Co magnets. Their luminescent colors were different. Thus, it is possible to distinguish between NdFeB and Sm–Co magnets by obtaining their CL images.

Neodymium–iron–boron (NdFeB) magnets have been used in various products such as electric vehicles and hard disk drives. Among rare-earth elements contained in NdFeB magnets, neodymium, dysprosium, and terbium are expected to be in short supply because of increasing demand. Thus, in the near future, it is expected that these rare-earth elements will need to be recovered from the existing stock of various kinds of magnets. Separation of NdFeB magnets from other magnets such as samarium–cobalt (Sm–Co) magnets is the first step in the recovery process. In the present study, we report a method to distinguish between NdFeB and Sm–Co magnets using a portable cathodoluminescence (CL) spectrometer that we previously realized [1-3]. The portable CL spectrometer detects luminescence emitted from insulating materials or semiconductors by the bombardment of electrons.

Figure 1 (a) shows a schematic of the portable CL spectrometer. The sample was bombarded with focused electrons by changing the temperature of a pyroelectric crystal of $LiTaO_3$ on which a gold wire was placed at 1 Pa. The luminescence of the sample was detected through a glass viewport using a commercially available camera whose built-in infrared filter was removed. The NdFeB and Sm–Co magnets were each dissolved in hydrochloric acid. Then, the iron in the solutions was removed using methyl isobutyl ketone, and the resulting solutions were dried in vacuum. The dried residues were used as samples.

Figures 1 (b) and (c) show CL images of the dried residues of the Sm–Co and NdFeB magnets, respectively, obtained with the portable CL spectrometer. The dried residue of the Sm–Co magnet produced orange luminescence. This color originated from the luminescent color of the samarium chloride, which has strong peaks at 597 and 647 nm. The dried residue of the NdFeB produced blue.

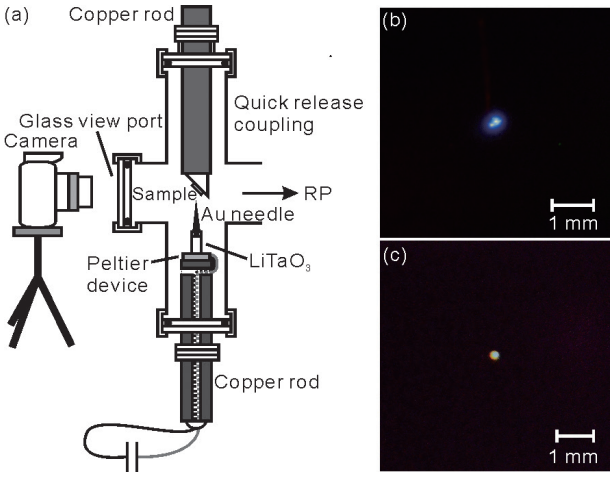

Fig. 1 (a) Schematic of a portable CL spectrometer. CL images of vacuum-dried residues of (b) Sm–Co magnet and (c) NdFeB magnet.

This luminescence was detected through a filter cut light with wavelengths less than 780 nm. Thus, this color was ascribed from the infrared luminescence of neodymium chloride, whose strongest peaks occur at 878 and 892 nm. The portable CL spectrometer can therefore distinguish between NdFeB magnets and Sm–Co magnets by the luminescent colors of their CL images.

References

[1] S. Imashuku and J. Kawai, Microsc. Microanl. **21**(S3), 793 (2015).

[2] S. Imashuku, I. Ohtani, and J. Kawai, Proceedings of ALC '15, 27p-P-48 (2015).

[3] S. Imashuku, K. Wagatsuma, and J. Kawai, Microsc. Microanl. **22**, 82 (2016).

Keywords: electron irradiation, spectroscopy, cathodoluminescence
Susumu Imashuku (Analytical Science Division)
E-mail: susumu.imashuku@imr.tohoku.ac.jp
URL: http://wagatsuma.imr.tohoku.ac.jp/

Biocompatibility of Ni- and Be-free Ti-based Bulk Metallic Glasses

Ti-based (Ti–Zr–Cu–Pd–Sn) bulk metallic glasses (BMGs) exhibited significant glass-forming ability, high strength, high thermal stability, low stress corrosion cracking susceptibility, and good bioactivity. *In vivo* implant evaluation showed that it had good tissue compatibility, equivalent bone integration, and the ability to bond with the Ti sample. It is thus possible to use Ti-based BMGs in biomedical applications.

Ti-based bulk metallic glasses (BMGs) are promising materials for applications in biomedical fields owing to their high corrosion resistance, excellent mechanical properties, and good biocompatibility. Many Ti-based BMGs have been developed in the framework of Ti–Ni–Cu and Ti–Zr–Cu–Ni alloy systems. However, these Ti-based BMGs contain Ni, Be, etc., which are unsuitable for use in the human body because of their cellular toxicity, limiting the application of Ti-based BMGs in biomedical fields. We developed Ni- and Be-free Ti–Zr–Cu–Pd BMGs with high strength and good corrosion resistance, showing that it is possible to create novel Ti-based BMG implants [1]. However, the relatively low glass-forming ability (GFA) (with a critical diameter of 7 mm) of these BMGs restricts their use in biomedical applications. Large critical diameters and excellent mechanical properties are fundamental requirements for such BMGs.

We investigated the influence of small amounts of additional elements on the formation and properties of Ti–Zr–Cu–Pd bulk glassy alloys. Minor Sn addition improved the glass-forming ability, thermal stability, and plasticity of the Ti–Zr–Cu–Pd alloy system [2]. The stress corrosion cracking (SCC) behavior in Hanks' solution and the bioactivity of Ti–Zr–Cu–Pd–Sn BMGs were also investigated. The results revealed that the Ti-based BMGs exhibited low SCC susceptibility in simulated body fluid. A bioactive calcium phosphate compound layer was obtained after two-step treatment on the Ti-based BMGs [3].

We implanted bars of the developed Ti–Zr–Cu–Pd–Sn BMG in the femoral bones of rats, followed by investigation of the local tissue reaction, as well as of local and whole-body component ion diffusion. After 12 weeks' implantation, inflammatory reactions, implant dislocation, or loosening were not observed in any of the cases. *In vivo* implant evaluation showed that the Ti-based BMG had good tissue compatibility, equivalent bone integration, and the ability to bond with the Ti sample (Fig. 1). No component ion diffusion was detected up to 3 months' post implantation (Fig. 2) [4]. Thus, the feasibility and efficacy of Ti-based BMGs for use as bone implants was confirmed.

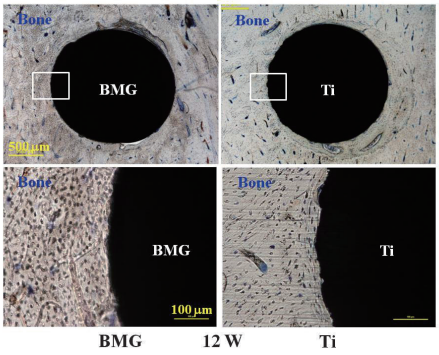

Fig. 1 Histological views of Ti-based BMG implant and Ti implant [4]. Both samples are well covered by surrounding bone tissue. There were no abnormal findings in the surrounding bone tissue. Objective magnification of the upper images is ×4 and that of the lower images is ×20.

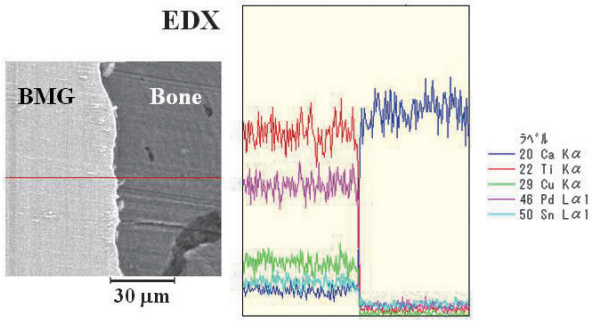

Fig. 2 EDX elemental analysis of implant border area [4]. No diffusion of any metallic ions in the BMG sample was found.

References

[1] S. L. Zhu, X. M. Wang, F. X. Qin, M. Yoshimura, and A. Inoue, Mater. Trans. **48**, 2445 (2007).

[2] S. L. Zhu, G. Q. Xie, A. Inoue, Z.D. Cui, X. J. Yang, and W. Zhang, Mater. Sci. Forum **833**, 79 (2015).

[3] F. X. Qin, S.L. Zhu, Z. H. Dan, A. Kawashima, and G. Q. Xie, J. Alloys Compd. **615**, S123 (2014).

[4] R. Kokubun, W. Wang, S. L. Zhu, G. Q. Xie, S. Ichinose, S. Itoh, and K. Takakuda, Bio-Med. Mater. Eng. **26**, 9 (2015).

Keywords: bulk metallic glass, biological, mechanical properties
Guoqiang Xie (Advanced Materials Development and Integration of Novel Structured Metallic and Inorganic Materials)
E-mail: xiegq@imr.tohoku.ac.jp
URL: http://amdi-pro.imr.tohoku.ac.jp/en/index.html

Positron–Monovacancy Interaction in d-Block Metals

Dr. Ishibashi is a core member of CMRI and has been conducting numerous studies based on positrons, which are known as powerful probes for detecting vacancy-type defects in various solids. Combined with theoretical calculations, it has become possible to identify defect species. The effect of a trapped positron on the monovacancy structure was systematically investigated. The present results are useful in predicting positron annihilation parameters accurately.

To describe the positron state in solids, Boroński and Nieminen proposed the two-component density-functional-theory formalism [1], with which interactions between a positron and electrons, as well as between a positron and nuclei, are explicitly described. In many practical calculations, a simplification is made assuming that the positron affects neither the electronic structure nor the atomic arrangement. This simplified scheme is called the "conventional scheme". The presence of a trapped positron affects the electronic structure and the atomic arrangement at a certain level, depending on the material being investigated. With both conventional and two-component DFT schemes, we recently calculated Doppler-broadening spectra and positron lifetimes for divacancies in C, Si, Ge, SiC, AlN, GaN, and InN, and we found that the difference between the two schemes depends on the bulk modulus [2]. For relatively soft materials, Si and Ge, the difference is significant. In the present study, we expanded our investigation to the positron–monovacancy interaction in d-block metals (except for Mn, Tc, and Hg) [3].

All the calculations were performed using our computational code QMAS (Quantum MAterials Simulator). In the conventional scheme, electronic structures, if necessary, and atomic positions are calculated independently of the presence of a positron. On the other hand, in the two-component scheme, electronic structures and atomic positions (when they are relaxed) are affected by the presence of a positron. Calculations were performed on supercells with sizes of 4 × 4 × 2 for hcp, 3 × 3 × 3 for fcc, and 4 × 4 × 4 for bcc. Further details are described in Ref. [3].

Figure 1 represents the positron density distribution trapped at a monovacancy in bcc Fe as an example of the obtained results. Differences between the positron lifetimes obtained by the two schemes, $\Delta\tau$, are plotted in Fig. 2 as a function of the atomic number, Z. For the unrelaxed structure, the positron lifetime calculated with the presence of a positron is generally longer than that obtained neglecting the positron effect. When the atomic positions are relaxed without the positron effect, for most cases, inward relaxation of the atoms surrounding the monovacancy is observed. However, this relaxation is suppressed when the positron effect is taken into account. Thus, the difference in the positron lifetime is widened, especially for the group V metals. As is the case for semiconductors, these differences are also related to the bulk modulus and the cohesive energy [3].

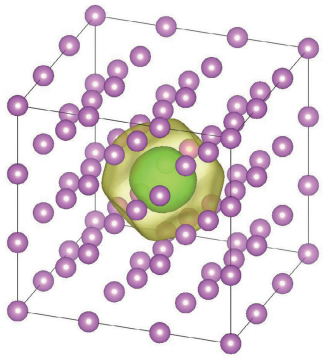

Fig. 1 Positron density distribution trapped at a monovacancy in bcc Fe. Two levels of isosurfaces are shown.

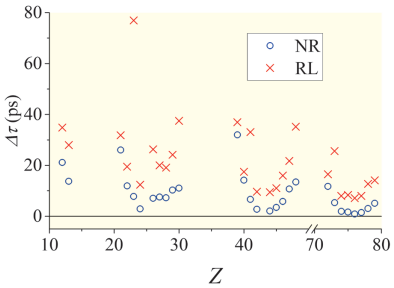

Fig. 2 Z-dependence of the differences in positron lifetimes trapped at a monovacancy, $\Delta\tau$, calculated with no relaxation (NR) and relaxation (RL).

References

[1] E. Boroński and R. M. Nieminen, Phys. Rev. B **34**, 3820 (1986).
[2] S. Ishibashi and A. Uedono, J. Phys.: Conf. Ser. **674**, 012020 (2016).
[3] S. Ishibashi, J. Phys. Soc. Jpn. **84**, 083703 (2015).

Keywords: positron annihilation, first-principles calculations, vacancy
Shoji Ishibashi [Research Center for Computational Design of Advanced Functional Materials (CD-FMat), AIST]
E-mail: shoji.ishibashi@aist.go.jp
Tetsuo Mohri (Project Leader of Computational Materials Research Initiative)
E-mail: tmohri@imr.tohoku.ac.jp